Electronic Supplementary Material (ESI) for Dalton Transactions.

Copper(II) complexes of a furan-containing aroylhydrazonic ligand: syntheses, structural studies, solution chemistry and interaction with HSA

Fagner da Silva Moura, Ygor S. Sobrinho, Carolina Stellet, Jilder D. P. Serna, Carolina B. P. Ligiero, Maurício I. Yoguim, Daphne S. Cukierman, Renata Diniz, Odivaldo C. Alves, Nelson H. Morgon, Aguinaldo R. de Souza, Nicolás A. Rey*

*nicoarey@puc-rio.br

Supplementary Information

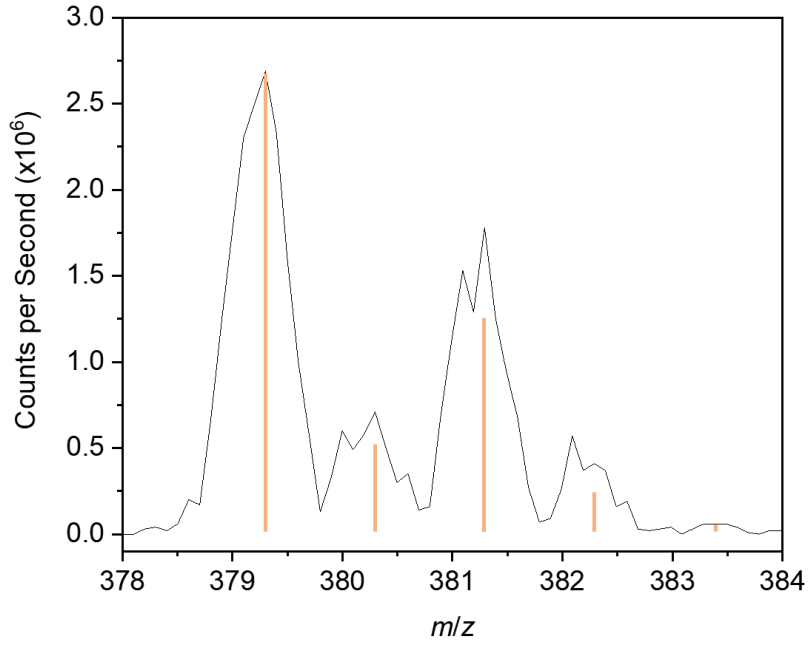

Figure S1. Experimental and calculated (vertical orange lines) isotope distribution pattern of the ESI-MS(+) peak related to the species [Cu(**HL**)DMF]$^+$.

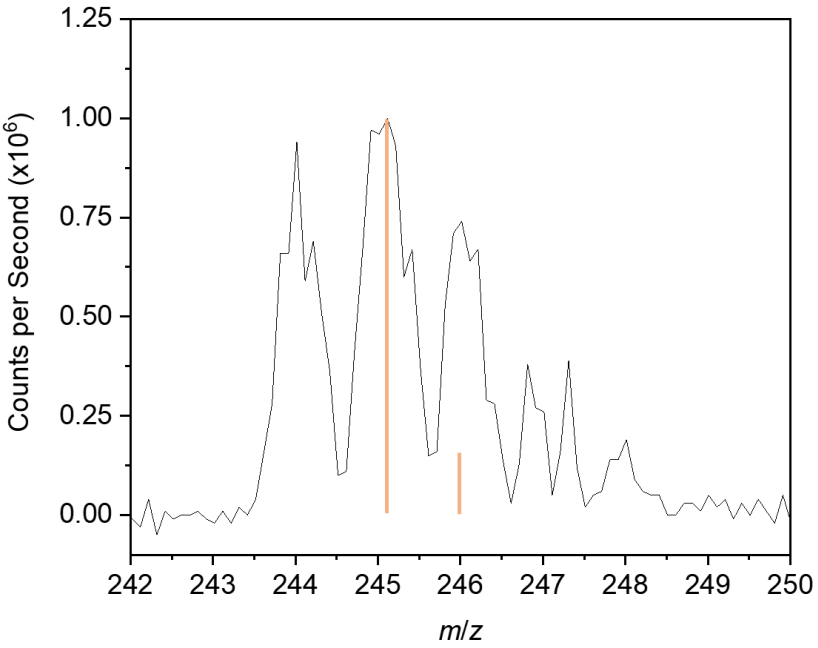

Figure S2. Experimental and calculated (vertical orange lines) isotope distribution pattern of the ESI-MS(+) peak related to the species [$\mathbf{H_2L}$+H]$^+$.

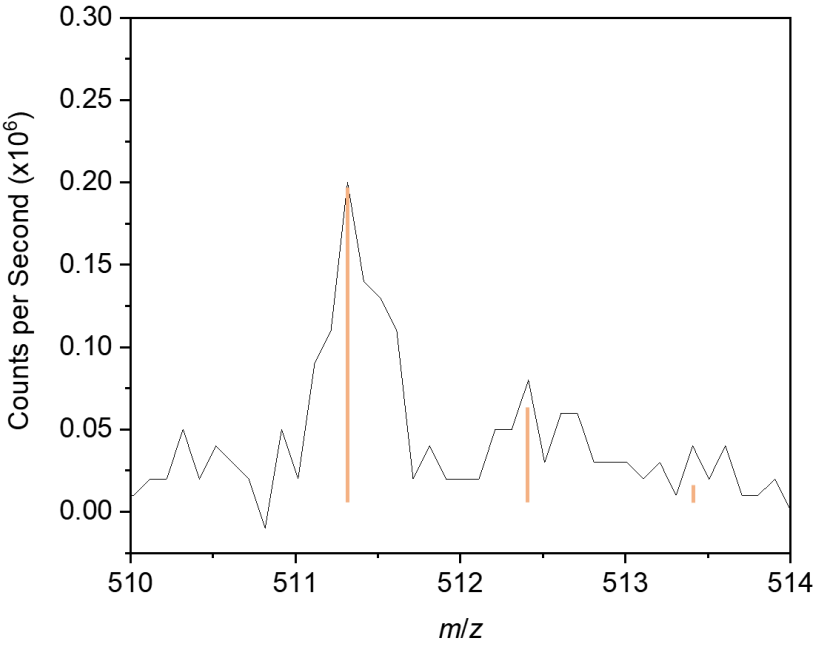

Figure S3. Experimental and calculated (vertical orange lines) isotope distribution pattern of the ESI-MS(+) peak related to the species $[2\mathbf{H_2L}+Na]^+$.

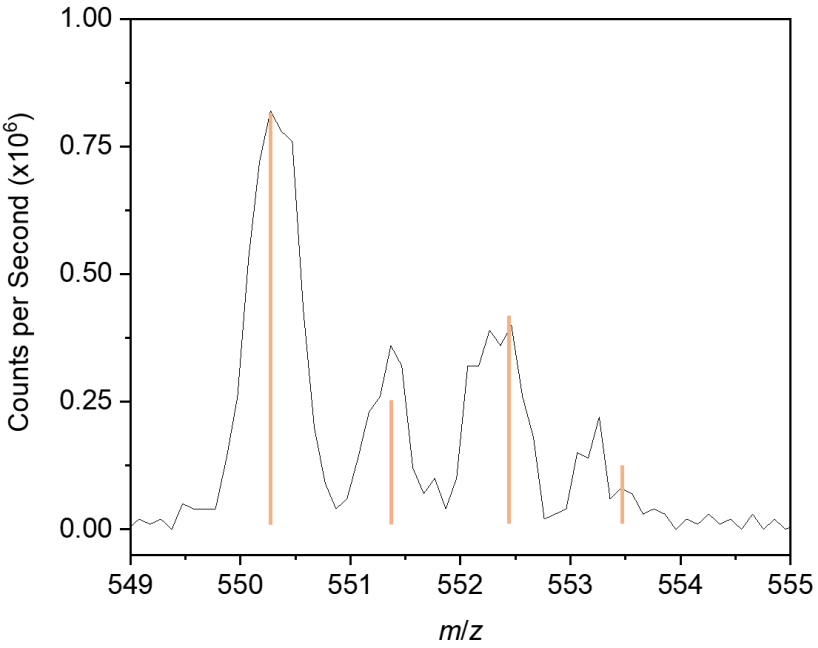

Figure S4. Experimental and calculated (vertical orange lines) isotope distribution pattern of the ESI-MS(+) peak related to the species $[Cu(\mathbf{HL})_2+H]^+$.

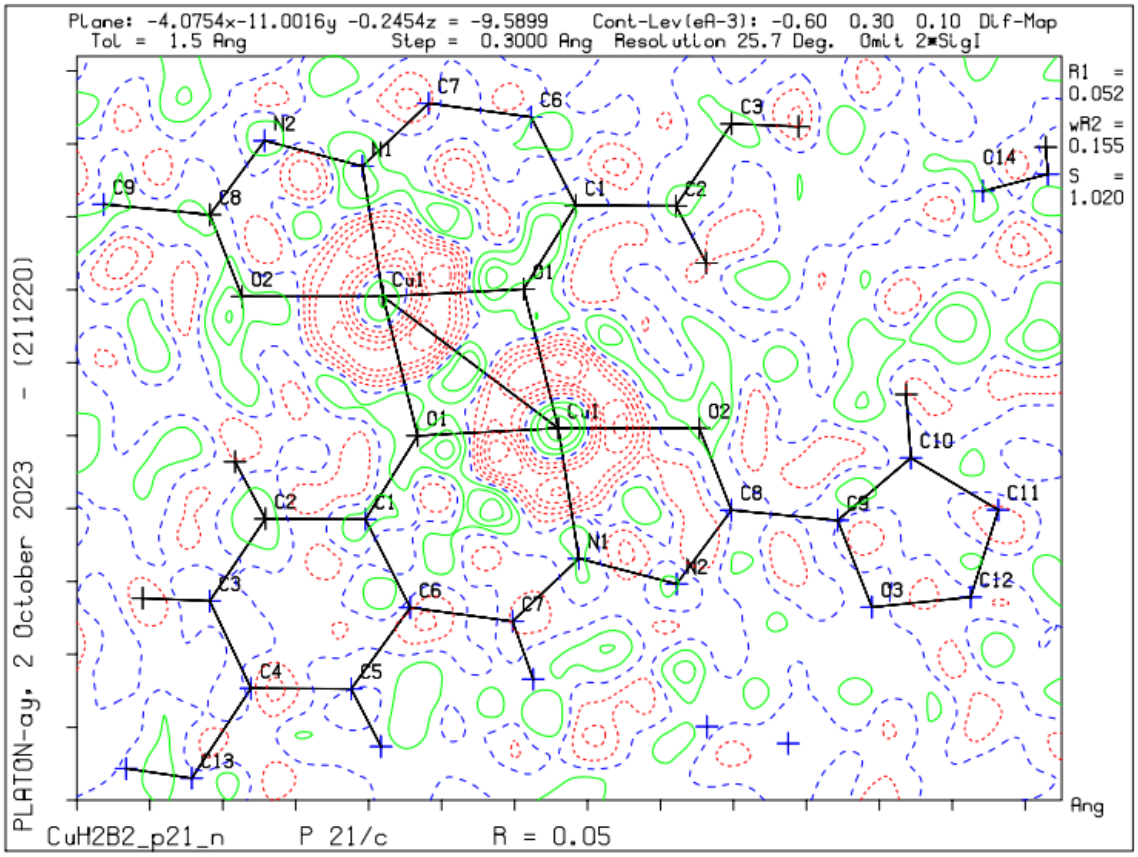

Figure S5. Fo-Fc map on the bis(μ-phenoxo)dicopper(II) motif plane of complex **2**.

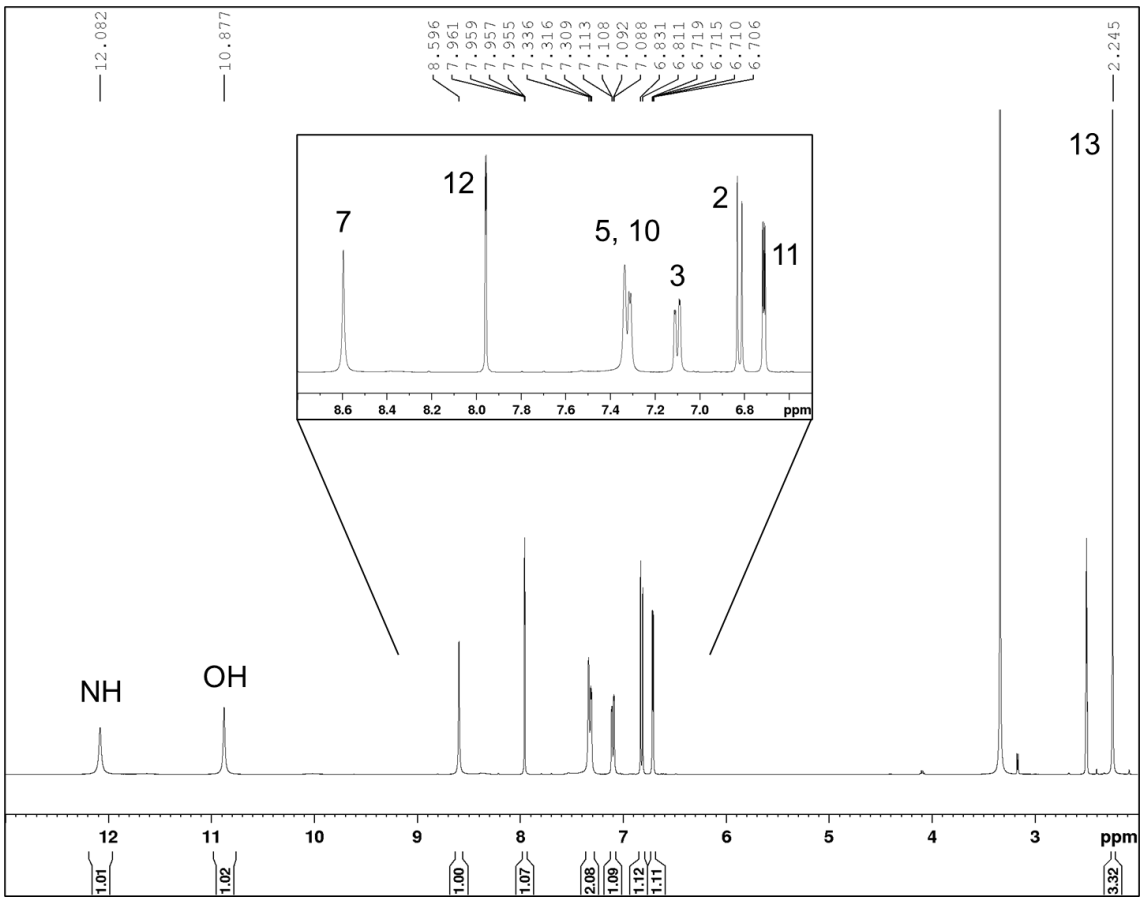

Figure S6. ^{1}H NMR spectrum (400 MHz) of **H_2L** in DMSO-d_6 at 298 K.

Table S1. Experimental crystallographic details for **H_2L** and its complexes **1** and **2**.

Crystal	**H_2L**	Complex **1**	Complex **2**
Chemical formula	$C_{13}H_{14}O_4N_2$	$C_{13}H_{13}O_4N_2ClCu$	$C_{32}H_{36}O_8N_4Cu_2$
*M*r (g mol^{-1})	262.26	360.24	731.73
Crystal system, space group	Orthorhombic, $P2_1\ 2_1\ 2_1$	Monoclinic, $P2_1/c$	Monoclinic, $P2_1/c$
Temperature (K)	296	293	296
a, *b*, *c* (Å)	4.9316(2), 12.4514(5),	12.6740(4), 6.9206(2),	6.2379(5), 14.5843(10),
β (°)	–	91.109(3)	94.394(2)
V (Å^3)	1273.49(9)	1416.74(7)	1595.39(2)
Z	4	4	2
Radiation type	Mo *K*α	Mo *K*α	Mo *K*α
μ (mm^{-1})	0.103	1.746	1.390
Crystal size (mm)	0.72 × 0.14 × 0.12	0.20 × 0.05 × 0.04	0.07 × 0.08 × 0.35
		Data collection	
Diffractometer	Bruker D8 Venture	Rigaku-Oxford-Diffraction	Bruker D8 Venture
Measured/Independent/Observed	22889, 2577, 2224	31799, 4009, 2953	25923, 3029, 2193
R_{int}	0.043	0.048	0.079
		Refinement	
$R[F^2 > 2\sigma(F^2)]$, $wR(F^2)$, S	0.040, 0.126, 1.09	0.035, 0.088, 1.04	0.052, 0.175, 1.21
No. of parameters	231	194	213
No. of restraints	238 (disorder in the furan ring)	0	0
Δρmax, Δρmin (e Å^{-3})	0.147, –0.150	0.414, –0.260	0.750, –0.640

Table S2. Selected bond distances for **H_2L**. DFT data [level of theory B3LYP/6-311++G(2d,p)] of the optimized structure in the gas phase were included for comparison.

Bond	XRD / Å	Calculated / Å
O1–C1	1.351(3)	1.342
O2–C8	1.237(3)	1.209
N1–C7	1.287(3)	1.284
N1–N2	1.379(3)	1.355
N2–C8	1.343(3)	1.388
C6–C7	1.443(3)	1.448

Table S3. Selected bond angles for **H_2L**. DFT data [level of theory B3LYP/6-311++G(2d,p)] of the optimized structure in the gas phase were included for comparison.

Angle	XRD / º	Calculated / º
C2–C1–O1	118.4(2)	118.1
C1–C6–C7	123.6(2)	121.8
C6–C7–N1	122.9(2)	121.7
C7–N1–N2	114.4(2)	119.0
N1–N2–C8	120.1(2)	119.8
N2–C8–C9	114.4(10)	112.8
N2–C8–O2	123.7(2)	123.6
C8–C9–O3	116.0(17)	115.9
C9–O3–C12	108.5(12)	107.1

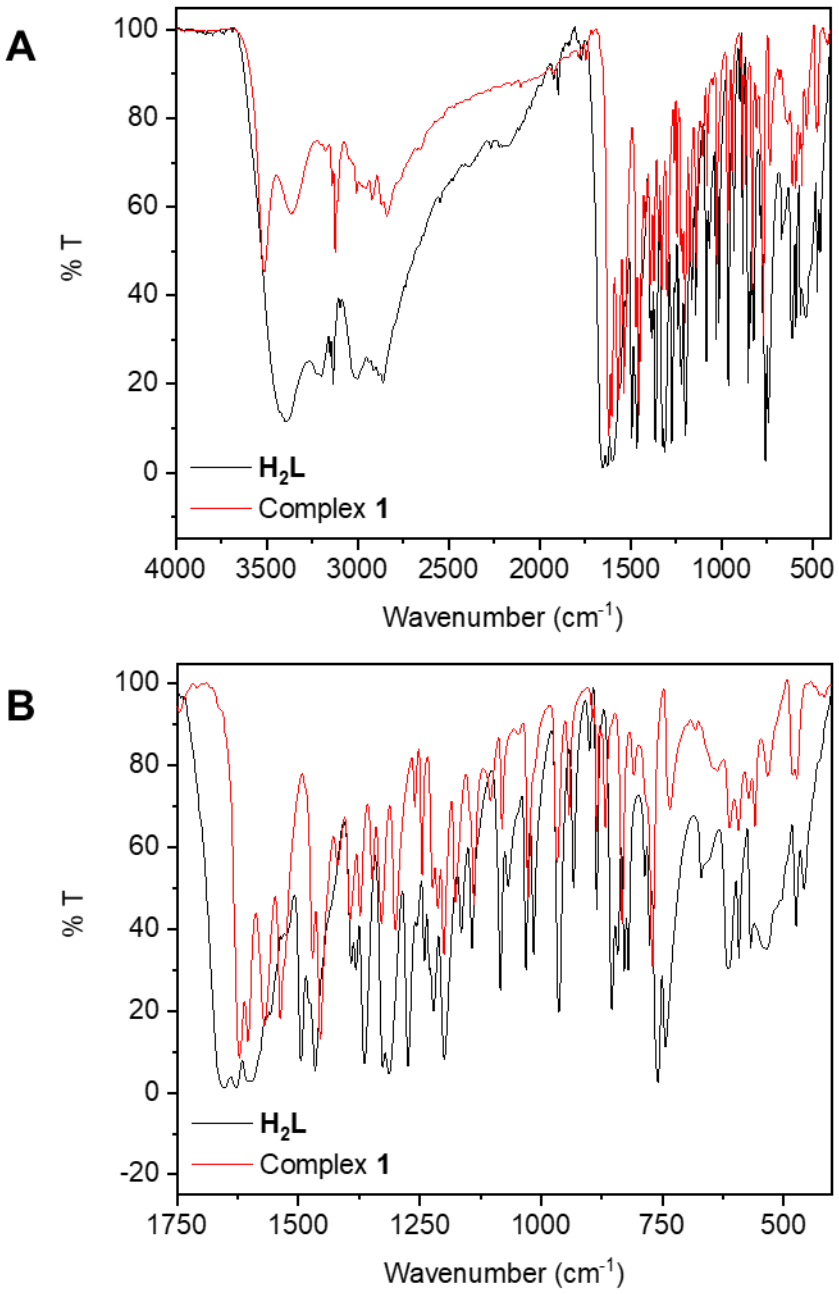

Figure S7. Overlapping of the mid-infrared spectra of **H_2L** and complex **1** in KBr, at room temperature, (**A**) from 4000 to 400 cm^{-1} and (**B**) expansion of the fingerprint region from 1750 to 400 cm^{-1}.

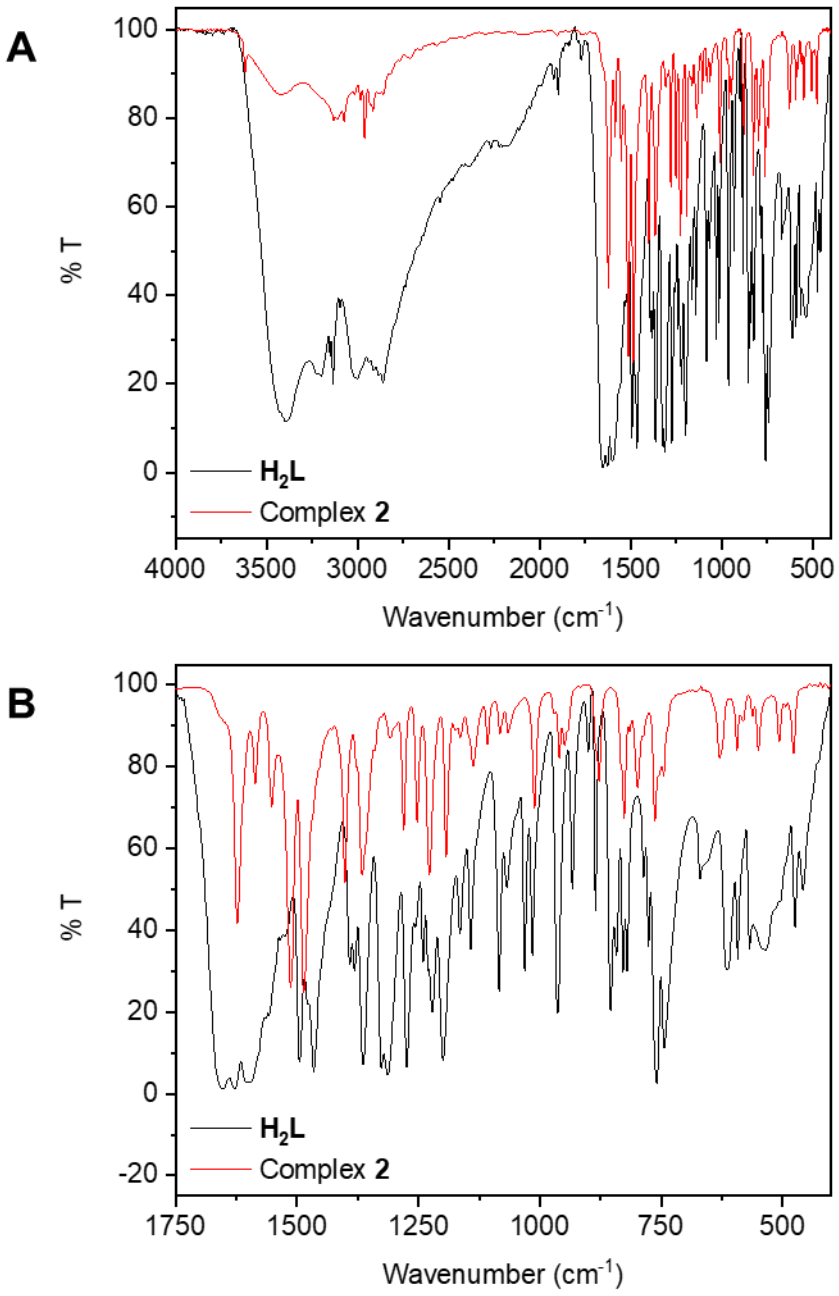

Figure S8. Overlapping of the mid-infrared spectra of **H_2L** and complex **2** in KBr, at room temperature, (**A**) from 4000 to 400 cm^{-1} and (**B**) expansion of the fingerprint region from 1750 to 400 cm^{-1}.

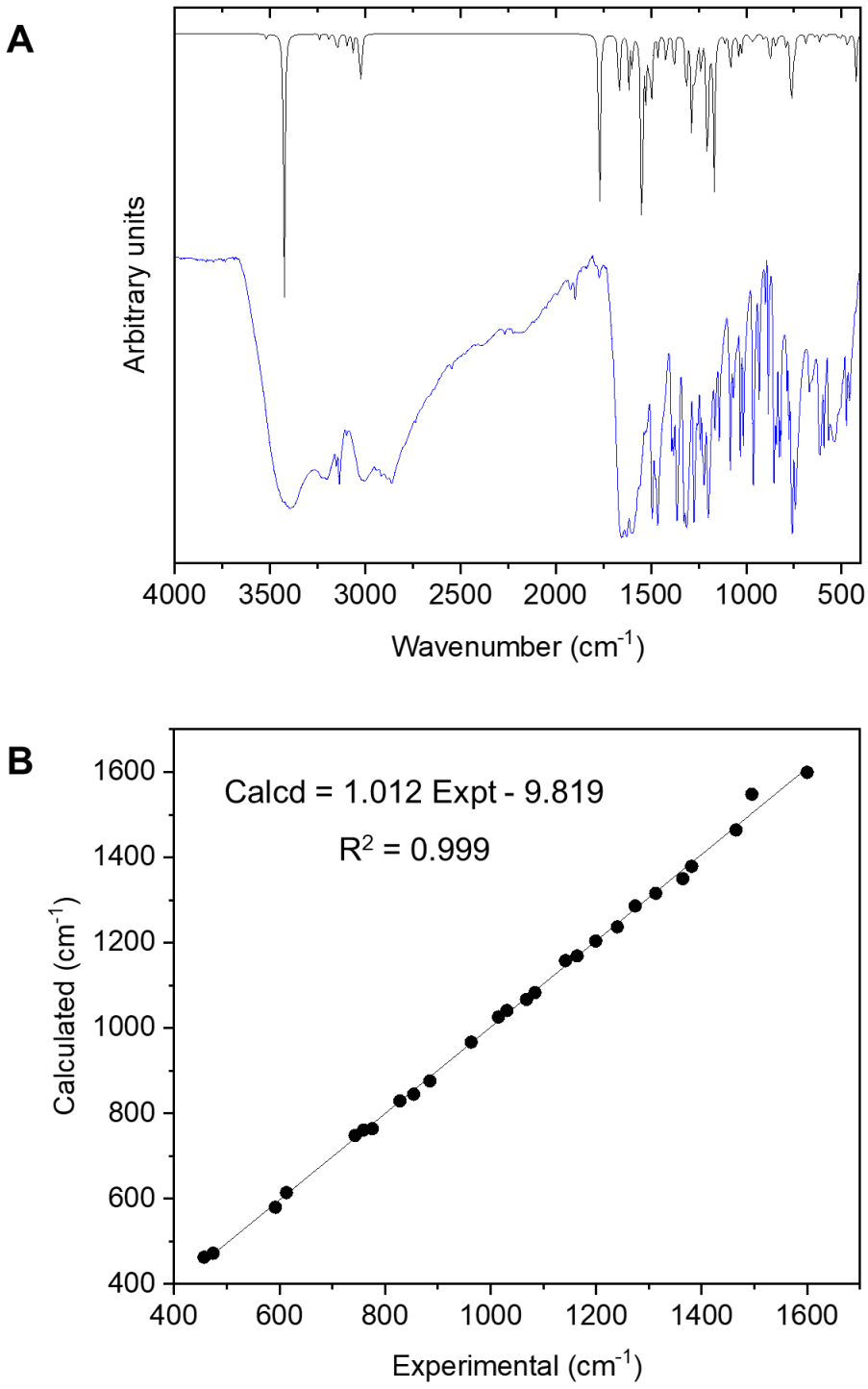

Figure S9. Mid-infrared spectra of **H_2L**. (**A**) Calculated (black) [gas phase, level of theory B3LYP/6-311++G(2d,p)] and experimental (blue) (KBr pellets at room temperature). (**B**) Plot of experimental *versus* calculated frequencies.

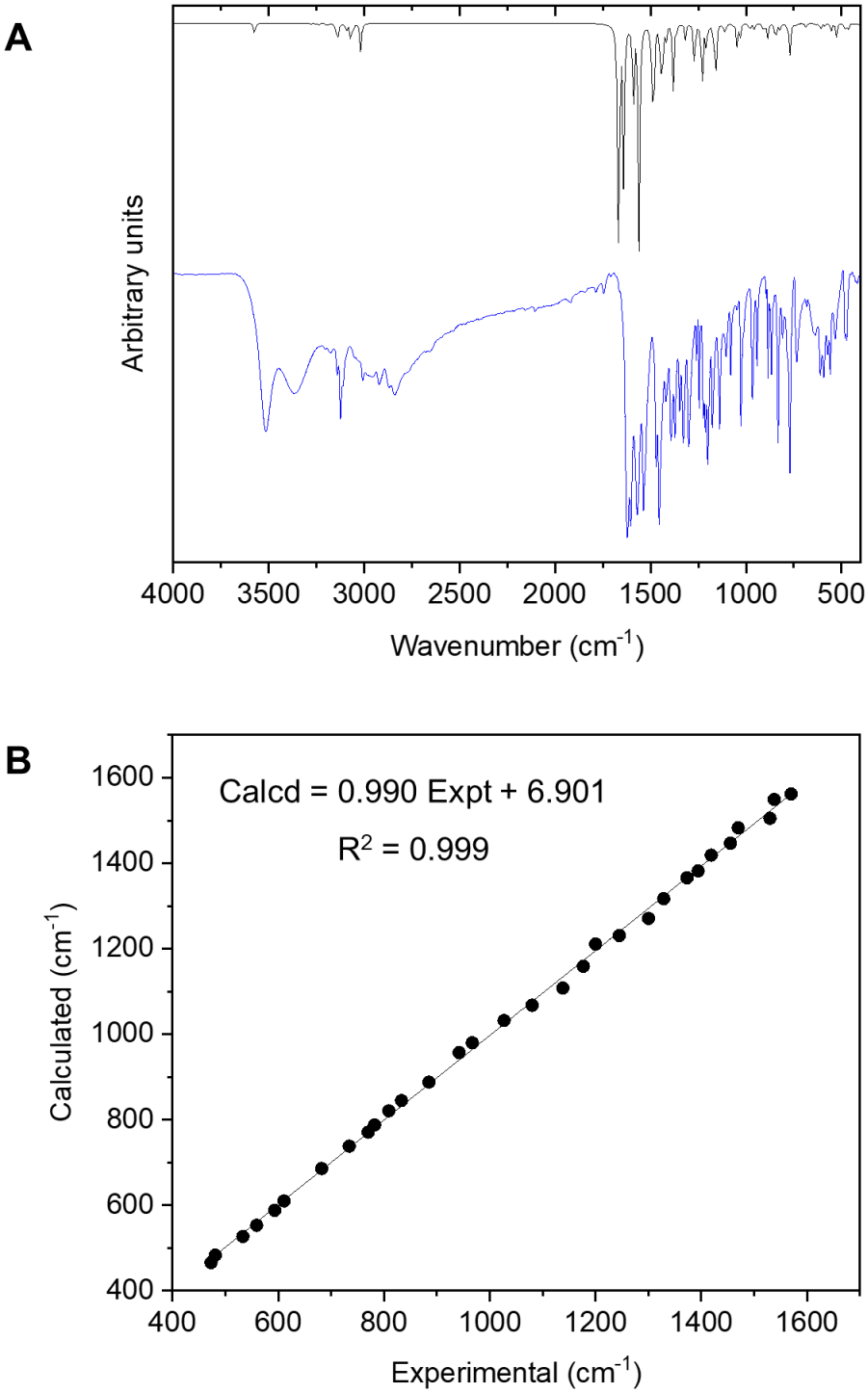

Figure S10. Mid-infrared spectra of complex **1**. (**A**) Calculated (black) [gas phase, level of theory B3LYP/6-311++G(2d,p)] and experimental (blue) (KBr pellets at room temperature). (**B**) Plot of experimental *versus* calculated frequencies.

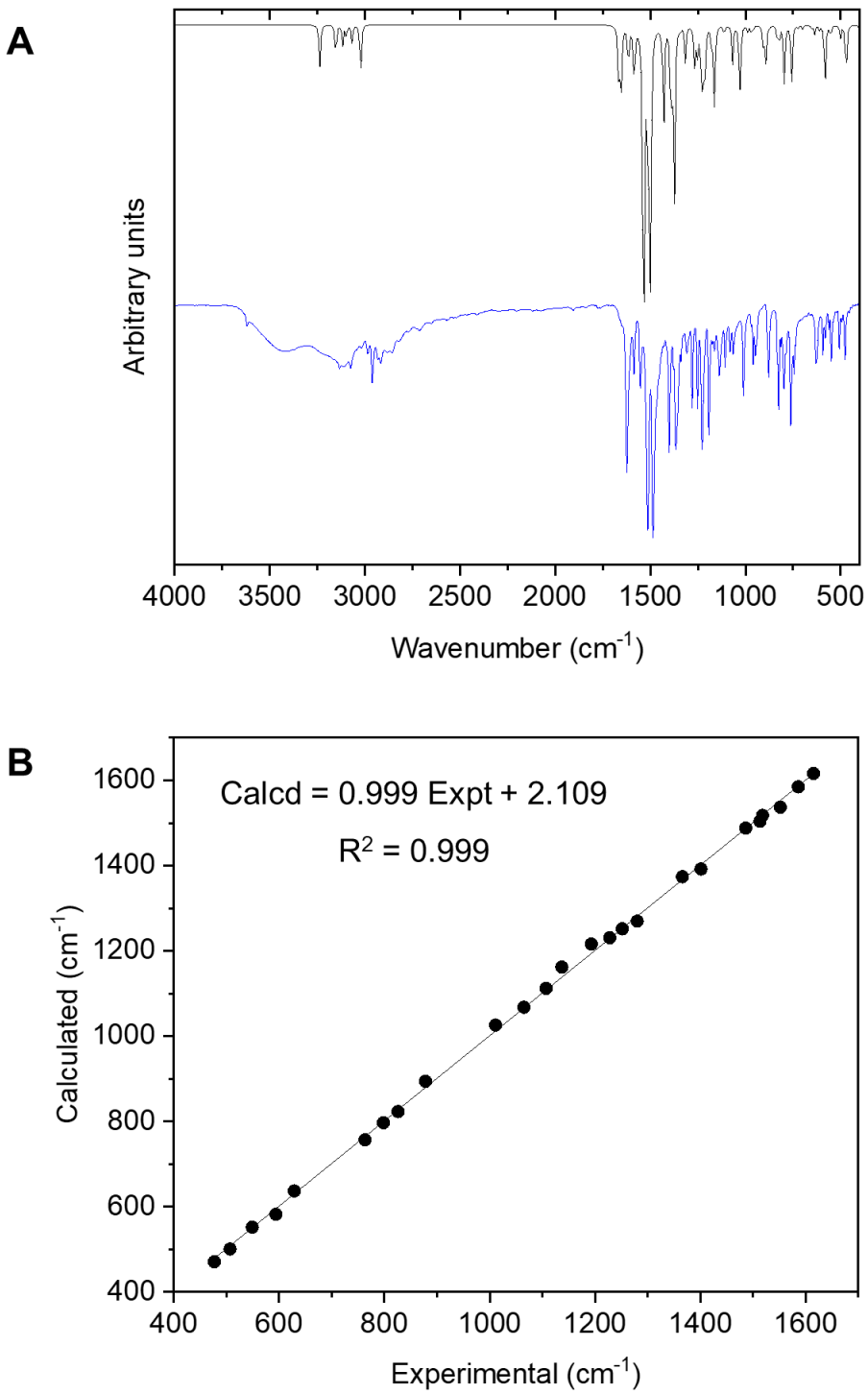

Figure S11. Mid-infrared spectra of complex **2**. (**A**) Calculated (black) [gas phase, level of theory B3LYP/6-311++G(2d,p)] and experimental (blue) (KBr pellets at room temperature). (**B**) Plot of experimental *versus* calculated frequencies. For the sake of simplicity, calculations involving complex **2** were performed disregarding the axial ligands.

Table S4. Experimental and calculated [gas phase, level of theory B3LYP/6-311++G(2d,p)] mid-IR data for the main absorptions related to the hydrazonic ligand **H_2L**, along with proposed assignments.

Experimental (cm^{-1})	Calculated (cm^{-1})	Assignment
3225	3519	ν(N–H)hydrazone
3202	3425	ν(O–H)phenol
3152	3154	ν(C–H)phenol
3136	3142	ν(C–H)phenol
3098	–	ν(C–H)
3017	3028	ν(C–H)azomethine
3002	–	ν(C–H)
2940	3094	ν_{as}(C–H)methyl
2914	3065	ν_{as}(C–H)methyl
2861	3020	ν_{sym}(C–H)methyl
1653**	1771	ν(C=O) + δ(N–N–H) hydrazone
1628**	1668	ν(C=N)hydrazone + ν(C=C)phenol ring
1600**	1599	ν_{as}(C=C)furan ring
1495*	1548	δ(C–N–H)hydrazone
1465*	1464	δ(C–O–H)phenol + δ(N–N–H)hydrazone
1381	1379	δ(OC–N–H) + δ(H–C=N) hydrazone
1364*	1350	ν(C=C)phenol ring + δ(H–C=N)hydrazone
1326*	–	ν(C–O)phenol
1313*	1316	δ(C=C–H)phenol + δ(H–C=N)hydrazone
1274*	1286	ν(C–O)furan + δ(OC–N–H)hydrazone
1240	1237	δ(C–O–H) + δ(C=C–H) phenol
1199*	1204	δ(C=C–H)furan + δ(N–N–H)hydrazone
1164	1169	ν(N–N) + δ(O–C–H)furan
1142	1158	δ(C=C–H)phenol
1084	1083	Furan breathing mode + δ(OC–N–H)hydrazone
1068	1067	δ(CH_3)
1031	1041	δ(C=C–H)furan
1015	1026	δ(CH_3)
963	967	$\delta_{out\text{-}of\text{-}plane}$(C–H)phenol + $\delta_{out\text{-}of\text{-}plane}$(C–H)azomethine
885	876	δ(C=C–O)furan + δ(O=C–N)hydrazone
854	845	$\delta_{out\text{-}of\text{-}plane}$(C–H)phenol + δ($CH_3$)
828	829	$\delta_{out\text{-}of\text{-}plane}$(C–H)furan
776	764	$\delta_{out\text{-}of\text{-}plane}$(C–H)furan + $\delta_{out\text{-}of\text{-}plane}$(O–H)phenol
759**	761	$\delta_{out\text{-}of\text{-}plane}$(O–H)phenol + $\delta_{out\text{-}of\text{-}plane}$(C–H)furan
743*	748	$\delta_{out\text{-}of\text{-}plane}$(O–H) + $\delta_{out\text{-}of\text{-}plane}$(C–H) phenol
613	614	$\delta_{out\text{-}of\text{-}plane}$(C–H)furan
592	580	$\delta_{out\text{-}of\text{-}plane}$(C–H) phenol + δ($CH_3$)
474	472	$\delta_{out\text{-}of\text{-}plane}$(N–H)hydrazone + δ(C=C–O)phenol
457	463	δ(C=C–C)phenol

** and * are the most intense bands

Table S5. Experimental and calculated [gas phase, level of theory B3LYP/6-311++G(2d,p)] mid-IR data for the main absorptions related to the mononuclear copper complex **1**, along with proposed assignments.

Experimental (cm^{-1})	Calculated (cm^{-1})	Assignment
3514*	3574	ν(N–H)hydrazone
3203	3238	ν_{as}(C–H)furan
3141	3148	ν_{as}(C–H)phenol
3124	3134	ν(C–H)phenol
3052	3072	ν(C–H)azomethine
3008	–	ν(C–H)
2922	3094	ν_{as}(C–H)methyl
2868	3060	ν_{as}(C–H)methyl
2840	3017	ν_{sym}(C–H)methyl
1622**	1666	ν(C=O) + ν(C=N) hydrazone
1604**	1641	ν(C=N) hydrazone + ν(C=O)
1570**	1562	δ(C–N–H)hydrazone
1538**	1549	ν(C=C)phenol ring
1530	1505	$\delta_{as}(CH_3)$
1470	1483	ν_{sym}(C=C)furan ring
1455**	1447	δ(C=C–C)phenol + δ(C=C–H)furan
1419	1419	$\delta_{sym}(CH_3)$
1394	1382	δ(H–C=N)hydrazone + δ(C=C–H)phenol
1373	1366	δ(C=C–H) + ν(C–O) phenol + δ(H–C=N)hydrazone
1329*	1317	δ(OC–N–H) + δ(H–C=N) hydrazone
1300*	1271	δ(C=C–H)phenol
1245	1231	δ(H–C=N) hydrazone + ν(C=C)phenol
1200*	1211	δ(C–N–H)hydrazone + δ(O–C–H)furan
1177	1159	δ(C=C–H)furan + δ(OC–N–H) + δ(C=C–H)phenol
1138	1108	ν(N–N)
1080	1068	$\delta(CH_3)$
1027	1032	$\delta(CH_3)$
967	980	δ(O–C–H)furan + $\delta(CH_3)$ + δ(C=C–H)phenol
942	957	$\delta_{out\text{-}of\text{-}plane}$(C–H)azomethine
885	888	δ(C=C–O)furan + δ(O=C–N)hydrazone
833*	845	$\delta_{out\text{-}of\text{-}plane}$(C–H)phenol + $\delta(CH_3)$
809	821	δ(C=C–C)phenol + $\nu(C–CH_3)$
782	788	Phenol breathing mode
770*	771	$\delta_{out\text{-}of\text{-}plane}$(C–H)furan
734	738	$\delta_{out\text{-}of\text{-}plane}$(C=O) + $\delta_{out\text{-}of\text{-}plane}$(C=C–H)furan
682	686	δ(C=C–C)phenol
611	610	$\delta_{out\text{-}of\text{-}plane}$(C=C–H)furan
593	588	**ν(Cu–N)** + δ(C=C–O)phenol
559	553	δ(OC–N–N)hydrazone
533	527	**ν(Cu–O2) + ν(Cu–O1)**
481	483	δ(C=C–C)phenol
473	466	**δ(O–Cu–N)**

** and * are the most intense bands

Table S6. Experimental and calculated [gas phase, level of theory B3LYP/6-311++G(2d,p)] mid-IR data for the main absorptions related to the dinuclear copper complex **2**, along with proposed assignments.

Experimental (cm^{-1})	Calculated (cm^{-1})	Assignment
3133	3153	ν_{as}(C–H)phenol
3108	3117	ν(C–H)azomethine
3076	–	ν(C–H)
2984	3097	ν_{as}(C–H)methyl
2916	3068	ν_{as}(C–H)methyl
2857	3022	ν_{sym}(C–H)methyl
1623*	1665	ν(C=N)hydrazone
1615	1616	ν_{as}(C=C)furan ring
1586	1585	ν_{as}(C=C)phenol ring
1552	1537	ν(OC–N) + ν(C=C)furan + δ(C=C–H)phenol
1518*	1518	δ(C=C–H)phenol
1513**	1504	δ(CH_3) + δ(C=C–H)furan + ν(C=O)hydrazone
1486**	1488	δ_{as}(CH_3)
1401*	1392	δ(H–C=N)hydrazone + δ(C=C–H)phenol
1366*	1374	δ(H–C=N)hydrazone + δ(C=C–H)furan
1280	1270	δ(H–C=N)hydrazone + δ(C=C–H)phenol
1252	1252	δ(C=C–H)furan
1228*	1231	ν(C–O)phenol + δ(C=C–H)phenol
1193*	1216	δ(O–C–H)furan + δ(C=C–H)phenol
1137	1162	δ(O–C–H)furan
1107	1112	δ(C=C–H)furan
1065	1068	ν(N–N) + δ(C=C–H)furan
1011	1026	δ(CH_3)
878	894	δ(O=C–N)hydrazone + δ(C=C–H)furan
826	823	$\delta_{out\text{-}of\text{-}plane}$(C–H)phenol + $\delta_{out\text{-}of\text{-}plane}$(C–H)furan
798	797	Phenol breathing mode
763*	757	$\delta_{out\text{-}of\text{-}plane}$(C–H)furan
629	637	$\delta_{out\text{-}of\text{-}plane}$(C–O–C)furan
594	582	**ν(Cu–O2)**
549	552	δ(OC–N–N)hydrazone + δ(C–C=N)azomethine
507	501	Phenol deformation mode
477	471	Bending of coordinated hydrazones

** and * are the most intense bands

In the region below 1620 cm^{-1}, the correlation between theory and experiment was remarkable for the three compounds, with a plot of experimental *versus* calculated frequencies giving straight lines of slopes 1.012 (**H_2L**), 0.990 (**1**) and 0.999 (**2**). The R^2 value for all of them was 0.999. In this spectral window, from 1620 to 400 cm^{-1}, the only computational failure observed was related to the phenol C–O stretching mode in **H_2L**, which could not be identified amongst the calculated vibrations. The program also failed in predicting accurately the methyl group stretching frequencies, systematically overestimating them. For **H_2L** and **1**, something similar happened with the ν(N–H) and ν(C=O) vibrations, while this is probably associated to the involvement of these groups in intermolecular H bonding with structural water molecules in the crystal, as evidenced by the XRD analysis. It is worth noting that intermolecular interactions were not considered during the DFT calculations. Specifically in the case of the ligand, phenol ν(O–H) and azomethine ν(C=N) modes were also miscalculated since they are involved in an intramolecular H bond. A similar fact was observed with the ν(C=N) vibration in complex **2**, overestimated by around 40 cm^{-1}.

Table S7. Main bands in the UV-Vis spectra of complexes **1** and **2**, along with their molar absorptivities.

Complex **1**		Complex **2**	
λ (nm)	**ε (L mol^{-1} cm^{-1})**	**λ (nm)**	**ε (L mol^{-1} cm^{-1})**
306	15,000 ± 200	308	27,700 ± 700
320	16,850 ± 150	320	33,450 ± 820
336	16,450 ± 150	336	32,150 ± 750
406	14,950 ± 200	404	30,900 ± 650
678	86 ± 1	630	190 ± 4

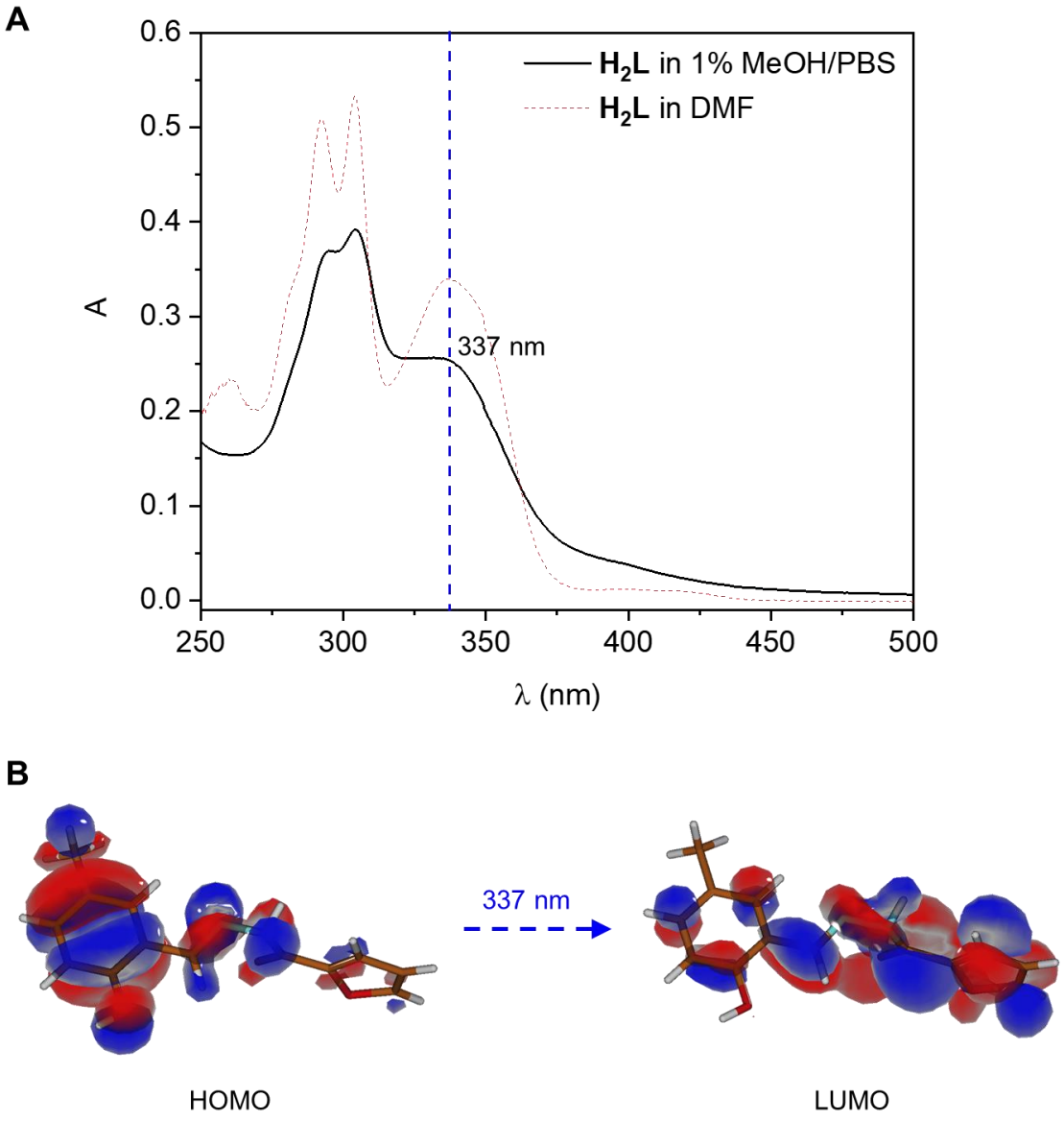

Figure S12. (**A**) UV-Vis spectra of ligand **H_2L** (2.0×10^{-5} mol L^{-1}) in 1% MeOH / PBS, pH 7.4 (black solid curve) and in DMF (red dotted curve), at r.t. Position of the HOMO-LUMO calculated transition is given as a dashed blue line (**B**) Frontier orbitals that take part in the process.

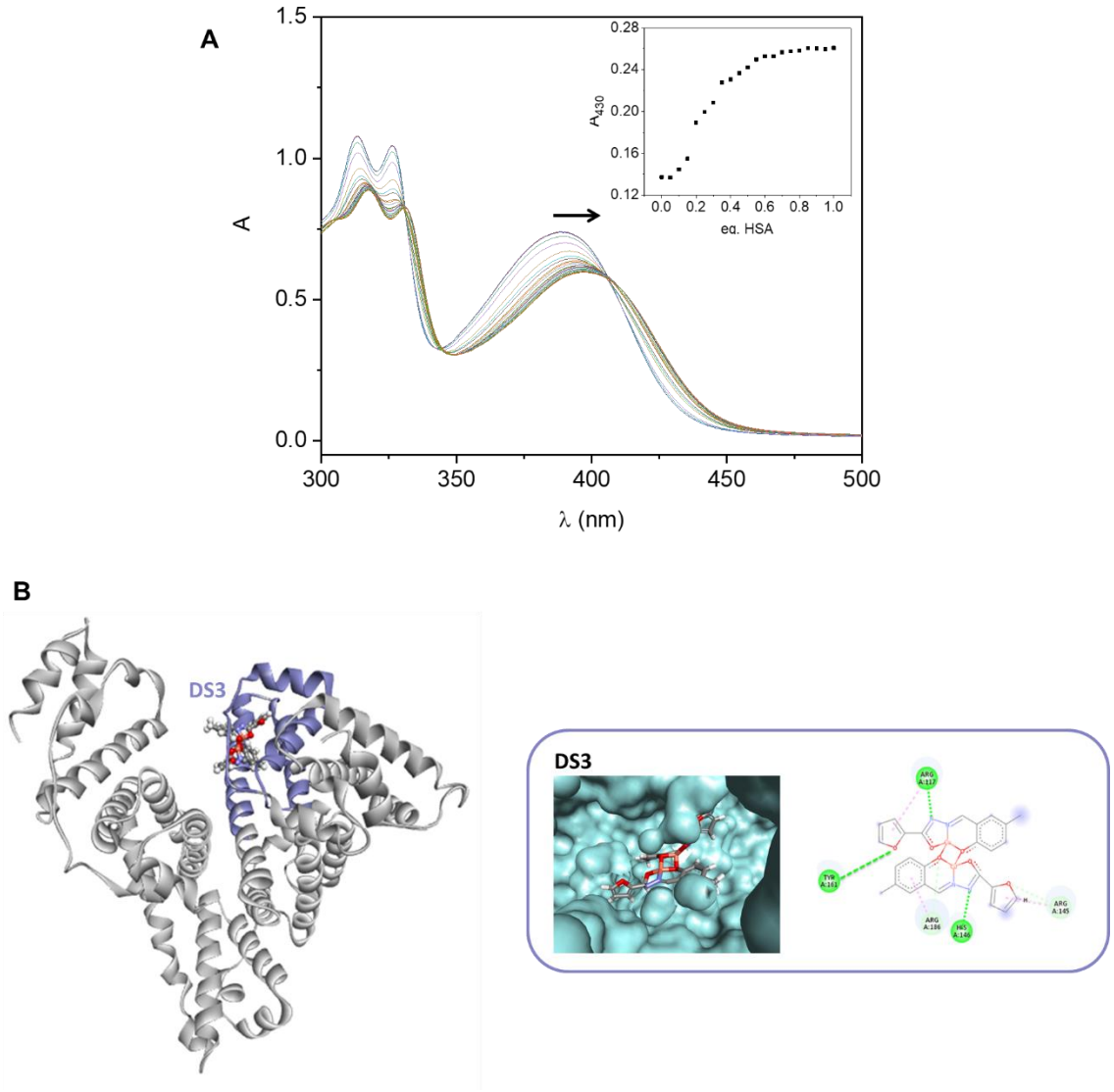

Figure S13. (**A**) UV-Vis titration of a 2×10^{-5} mol L^{-1} solution of **2** (2% MeOH / PBS, pH 7.4) with HSA at 25 ºC. *Inset*: absorbance at 430 nm as a function of HSA equivalents. (**B**) Molecular docking results with indication of pose and most probable interactions of the neutral, dimeric complex **2** at the DS3 site.